

A search for evidence of small-scale inhomogeneities in dense cores from line profile analysis

Lev Pirogov

Institute of Applied Physics, Russian Academy of Sciences, Ulyanova 46, Nizhny Novgorod, Russia;
pirogov@appl.sci-nnov.ru

Received 2018 January 29; accepted 2018 April 12

Abstract In order to search for intensity fluctuations on the HCN(1–0) and HCO⁺(1–0) line profiles, which could arise due to possible small-scale inhomogeneous structure, long-term observations of high-mass star-forming cores S140 and S199 were carried out. The data were processed by the Fourier filtering method. Line temperature fluctuations that exceed the noise level were detected. Assuming the cores consist of a large number of randomly moving small thermal fragments, the total number of fragments is $\sim 4 \times 10^6$ for the region with linear size ~ 0.1 pc in S140 and $\sim 10^6$ for the region with linear size ~ 0.3 pc in S199. Physical parameters of fragments in S140 were obtained from detailed modeling of the HCN emission in the framework of the clumpy cloud model.

Key words: lines: profiles — molecular data — methods: data analysis — ISM: clouds — ISM molecules — ISM: structure — ISM: individual objects (S140)

1 INTRODUCTION

The regions where high-mass stars and stellar clusters are born are highly turbulent and inhomogeneous (e.g., Tan et al. 2014). The extent of turbulence is enhanced in the vicinities of massive stars where gas due to various kinds of instabilities could fragment into small-scale structures down to the scales unresolved by modern instruments. There is a great deal of indirect evidence for the existence of small-scale unresolved inhomogeneities (fragments, clumps) in regions of high-mass star formation. This follows from the fact that the observed molecular line profiles of different species are close to Gaussian profiles without signs of saturation and their widths are much higher than thermal ones (e.g. Kwan & Sanders 1986). Nearly constant volume densities in clouds with strong column density variations (e.g. Bergin et al. 1996) and detection of C I emission over large areas correlated with molecular maps (e.g. White & Padman 1991; Kamegai et al. 2003) also imply a small-scale clumpy structure.

Important evidence for the existence of small thermal fragments in high-mass star-forming regions is provided by anomalies in relative intensities of the hyperfine components in HCN(1–0). This effect is connected with an overlap of thermally broadened profiles for closely located hyperfine components in the higher HCN rotational

transitions (mainly, $J = 2 - 1$) and is efficient at kinetic temperatures $\gtrsim 20$ K (Guilloteau & Baudry 1981). Yet, if the local profiles are broadened by microturbulence and are suprathermal as in high-mass star-forming cores ($\gtrsim 2$ km s^{−1}), it becomes practically impossible to reproduce the observed HCN(1–0) anomalies in the framework of the microturbulent model (Pirogov 1999). On the other hand, if the cores consist of small thermal fragments with low volume filling factor moving randomly with respect to each other, the observed HCN(1–0) profiles with intensity anomalies and high linewidths can be easily reproduced (Pirogov 1999).

If the observed line profile is a sum of profiles of randomly moving fragments, one should expect intensity fluctuations to exist due to fluctuations in the number of fragments along the line of sight at distinct velocities. Martin et al. (1984) derived an analytical expression for molecular line emission of a cloud consisting of a large number of small identical fragments and Tauber (1996) obtained an expression for the standard deviation of line intensity fluctuations due to such a structure. Using their approach, it is possible to derive parameters of a small-scale structure from observations, mainly the total number of fragments in a telescope beam.

Previously, we performed long-term observations in various molecular lines (HCN(1–0), CS(2–1), ¹³CO(1–

0), HCO⁺(1–0) and some others) of high-mass star-forming cores which show HCN(1–0) hyperfine anomalies (S140, S199, S235) and photodissociation regions (Orion, W3) (Pirogov & Zinchenko 2008; Pirogov et al. 2012). We detected residual fluctuations on line profiles and estimated the total number of thermal fragments in a beam using an analytical approach. By comparing the results of detailed calculations of line emission in a framework of the model that consisted of identical thermal fragments (clumpy model) with the observed nearly Gaussian HCN(1–0) profiles, estimates of sizes and densities of fragments were obtained for S140 and S199. Yet, these results suffered from the drawback connected with arbitrarily chosen parameters for the method of extracting residual intensity fluctuations from line profiles. In this paper, based on the report given at the All-Russian Astronomical Conference VAK-2017 (Samus & Li 2018), new higher quality observational results for the cores S140 and S199 in HCN(1–0) and HCO⁺(1–0) lines are presented. The lines in these objects have nearly Gaussian profiles, which is important for comparison with the results of the clumpy model calculations. To estimate standard deviations of residual line intensity fluctuations that could be due to small-scale clumpy structure, a new Fourier filtering method is used. This approach helped to recalculate parameters of the small-scale structure including the total number of fragments in the beam for S140 and S199 and physical parameters of fragments for S140.

2 ANALYTICAL MODEL

Considering a model cloud that consists of identical randomly moving fragments with a low volume filling factor and assuming that the velocity dispersion of fragment motions (σ) is much higher than the inner velocity dispersion (v_0), Martin et al. (1984) obtained an expression for a cloud’s optical depth (τ) which is proportional to N_c , the number of fragments in a column with the cross-sectional area of a single fragment. Using this approach for $N_c \lesssim 10$, Tauber (1996) derived an expression which can be written as follows

$$\frac{\Delta T_R}{T_R} = \frac{\tau}{(e^\tau - 1)\sqrt{K N_{\text{tot}} \frac{v_0}{\sigma}}}, \quad (1)$$

where ΔT_R is a standard deviation of fluctuations of line radiation temperature in some range near the line center, T_R is a peak line radiation temperature and K is a factor depending on the optical depth distribution within a fragment. For the Gaussian distribution, K is equal to 1. For the case of opaque discs, it is equal to π . Since the contribution of emission from an ensemble of small

fragments is statistically independent of atmospheric and instrumental noise, a standard deviation of temperature fluctuations due to small fragments can be calculated as: $\Delta T_R = \sqrt{\Delta T_L^2 - \Delta T_N^2}$, where ΔT_L and ΔT_N are the observed standard deviations of temperature fluctuations within and outside the line profile range, respectively. Thus, knowing ΔT_R , T_R , kinetic temperature and line optical depth (τ), it is possible to estimate a number of thermal fragments in the beam (N_{tot}). Yet, in order to detect radiation temperature fluctuations due to such a structure, observations with high signal-to-noise ratio and with high spectral resolution are needed. Another problem with this approach is connected with the correct measurement of ΔT_R .

3 THE RESULTS OF OBSERVATIONS

We carried out observations of two high-mass star-forming cores, S140 and S199, in the HCN(1–0) line at 88.6 GHz with the Institut de Radioastronomie Millimétrique-30m (IRAM-30m) telescope in 2010 and in the HCN(1–0) and HCO⁺(1–0) lines (at 88.6 GHz and 89.2 GHz, respectively) with the Onsala Space Observatory-20m (OSO-20m) telescope in 2017. In addition, we observed these sources in the H¹³CN(1–0) and H¹³CO⁺(1–0) lines with the OSO-20m telescope in 2017. The IRAM-30m beam at these frequencies is $\sim 29''$ and the OSO-20m beam is $\sim 41''$. System noise temperatures were $\sim 130 - 180$ K and $\sim 170 - 240$ K, and frequency resolutions were 39 kHz and 19 kHz in the IRAM-30m and OSO-20m observations, respectively. After several hours of integration in frequency switching mode, the noise rms was ~ 0.01 K and ~ 0.02 K for the IRAM-30m and OSO-20m observations, respectively. The observed profiles towards S140 and S199 contain a “quiet” nearly Gaussian component (line widths ~ 2.5 km s^{–1}) and a high-velocity wing emission with lower amplitude. For the purpose of our analysis, high-velocity components were subtracted. The source coordinates, distances and linear resolutions at ~ 89 GHz are given in Table 1.

In order to estimate standard deviations of radiation temperature fluctuations on line profiles that could be due to small-scale structure (ΔT_R), it is necessary to correctly remove the main component from line profiles. As was pointed out by Tauber (1996), one of the possible methods is to do Fourier high-pass filtering. This method is based on the idea that a small-scale structure should produce a much broader Fourier (power) spectrum than the main line profile. After filtering, a noise-like residual spectrum, probably with different standard deviations within and outside the line range, is obtained.

Table 1 Source List

Source	$\alpha(2000)$ (^h) (^m) (^s)	$\delta(2000)$ ([°]) ([']) (^{''})	D (pc)	Linear Resolution (pc)
S140 (L1204)	22 19 18.4	63 18 45	764(27) (Hirota et al. 2008)	~ 0.11 (IRAM-30m) ~ 0.15 (OSO-20m)
S199 (IC1848)	03 01 32.3	60 29 12	2200(200) (Lim et al. 2014)	~ 0.3 (IRAM-30m)

Previously (Pirogov & Zinchenko 2008; Pirogov et al. 2012) we used this method taking arbitrary filter boundaries to reject harmonics of power spectra corresponding to the main line profile.

In Figure 1 the observed profiles and the corresponding power spectra are shown on the left and right panels, respectively. The power spectra contain features with low amplitudes at inverse velocities higher than the main Gaussian profile ranges ($> 0.4 - 0.5$ (km s⁻¹)⁻¹), implying small deviations from the Gaussians. Fitting the observed profiles by 2–3 overlapping Gaussians (or triplets in the case of HCN) with suprathermal widths, it is possible to reproduce some of the low-amplitude features for inverse velocities up to ~ 0.7 (km s⁻¹)⁻¹ (Fig. 1, right panels). The spectral features at higher inverse velocities could be attributed to the small-scale clumpy structure as well as to atmospheric and instrumental noise.

4 FOURIER FILTERING AND THE $\Delta T_R(F_{\text{EFF}})$ DEPENDENCIES

In order to select an optimal boundary for the high-pass Fourier filter (F_{eff}), the filtering has been done for different values of F_{eff} from 0.7 to 2 (km s⁻¹)⁻¹ and the ΔT_R values have been calculated for the 3 km s⁻¹ line range of the observed HCN(1–0) and HCO⁺(1–0) profiles (23 and 46 velocity channels for the IRAM-30m and OSO-20m data, respectively). The results for S140 (OSO-20m) are shown in Figure 2 (left). There is a sharp decrease in ΔT_R with increasing F_{eff} . For $F_{\text{eff}} \gtrsim 1.3$ (km s⁻¹)⁻¹ the dependencies become nearly linear. Similar behavior is found for the IRAM-30m data.

For comparison, we performed test calculations of the HCN and HCO⁺ excitation in the framework of a model cloud that consisted of identical thermal fragments with small volume filling factors moving randomly with respect to each other with random velocities having a Gaussian distribution. The line profile from each fragment is a Gaussian with thermal width. A simplified version of the 1D clumpy model described previously (Pirogov 1999, Appendix; Pirogov & Zinchenko 2008) is used. The model matches the conditions of the analytical approach and the model line intensities and widths are close to the observed ones for S140. In order to speed up test calculations, the number of fragments in the mod-

els was reduced. This led to higher values of model ΔT_R compared with the observed ones.

By varying the initial values of the random number generator, one could change the spatial distribution and velocities of fragments. We performed a hundred runs with different randomly-generated initial values for two HCN and one HCO⁺ test models, and processed the results in the same way as the data from observations, namely, by filtering corresponding power spectra for different F_{eff} values and calculating ΔT_R for the 3 km s⁻¹ line range.

There is a scatter in the ΔT_R model values from one model run to another. For each F_{eff} , the mean ΔT_R value and dispersion have been calculated and the resulting $\langle \Delta T_R \rangle (F_{\text{eff}})$ dependencies are plotted in Figure 2 (right). They are close to linear and the $\langle \Delta T_R \rangle$ value at $F_{\text{eff}} = 0.7$ (km s⁻¹)⁻¹ is nearly equal to the analytical estimate calculated from Equation (1) for the case of opaque discs. The $\Delta T_R(F_{\text{eff}})$ dependencies for individual model runs are also found to be more or less linear.

Therefore, it is probable that the values of ΔT_R for $F_{\text{eff}} \lesssim 1.3$ (km s⁻¹)⁻¹ for S140 and $\lesssim 1$ (km s⁻¹)⁻¹ for S199 are enhanced by some structures (processes) other than randomly distributed thermal fragments (e.g. gravitationally bounded compact cores, “tangled structures” (Hacar et al. 2016) or “cloudlets” (Tachihara et al. 2012)). In order to get an unbiased estimate of ΔT_R associated with thermal fragments, we calculated linear regressions for the observed $\Delta T_R(F_{\text{eff}})$ dependencies in the range where dependencies are nearly linear and extrapolated them to lower F_{eff} . Regression lines are shown in Figure 2 (left). We took the ΔT_R values calculated from regression lines at $F_{\text{eff}} = 0.7$ (km s⁻¹)⁻¹ as standard deviations of line temperature fluctuations produced by randomly distributed thermal fragments in the beam. The uncertainty of these estimates is assumed to be the same as the uncertainty in the model calculations ($\sim 25\%$).

5 TOTAL NUMBER OF FRAGMENTS IN THE BEAM

Knowing ΔT_R , T_R , line width, optical depth and kinetic temperature, it is possible to derive the total number of thermal fragments (N_{tot}) within the telescope beam from

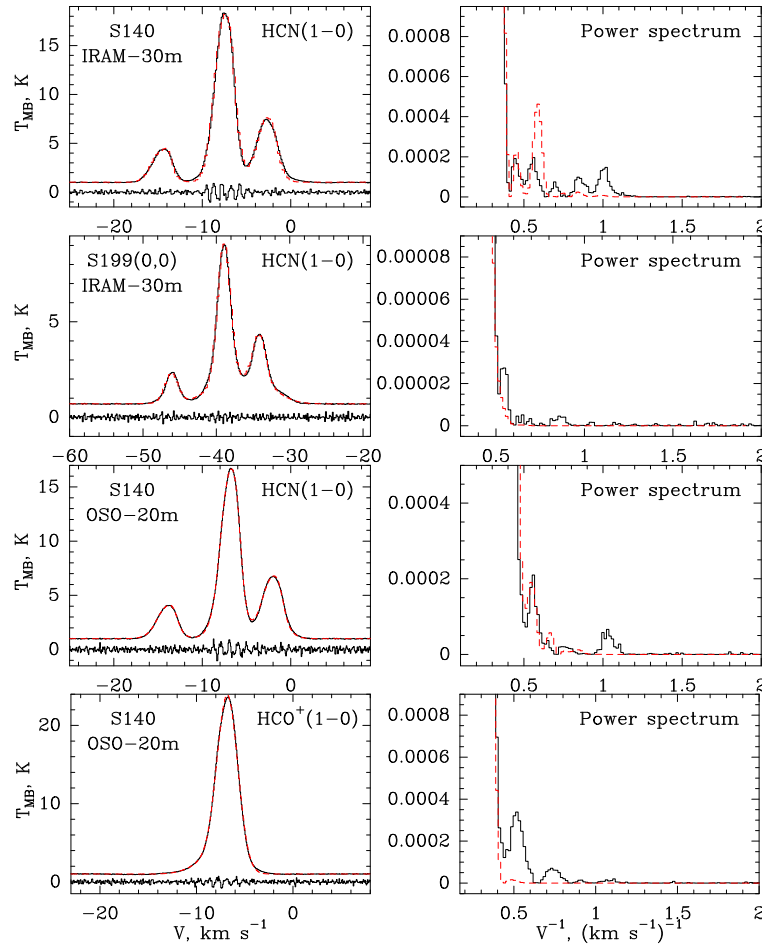


Fig. 1 The observed HCN(1–0) and HCO⁺(1–0) profiles in S140 and in S199 (*left panels*) and the corresponding power spectra (Fourier transform) for low amplitudes (*right panels*). Residual noise obtained after filtering power spectra with arbitrary value $F_{\text{eff}} = 1 \text{ (km s}^{-1}\text{)}^{-1}$ and multiplied by a factor of 10 is shown under the observed profiles. *Red dashed curves* correspond to the fits by overlapping Gaussian functions (triplets in the case of HCN(1–0)) and their power spectra.

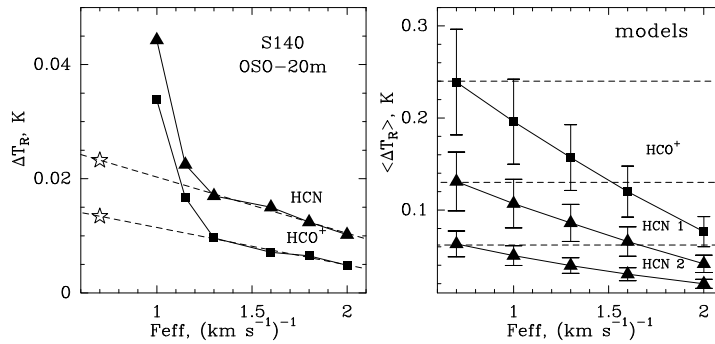


Fig. 2 The standard deviations ΔT_R calculated for the observed (*left*) and model (*right*) HCN(1–0) and HCO⁺(1–0) profiles for different F_{eff} values. The model ΔT_R values are the mean values of a hundred model runs and error bars denote their standard deviations. The *dashed lines* in the right panel correspond to analytical estimates of ΔT_R derived from Equation (1). Stars on the left panel represent the ΔT_R values taken for calculations of total number of fragments in the beam.

Equation (1). Kinetic temperatures (T_{KIN}) for S140 and S199 are taken close to the estimates from Malafeev et al. (2005) and Zinchenko et al. (1997), respectively. Optical depths (τ) are calculated from a comparison of

the HCN(1–0) and HCO⁺(1–0) line widths with the optically thin H¹³CN(1–0) and H¹³CO⁺(1–0) line widths. For the case of HCN(1–0), τ is an optical depth of the $F = 2 - 1$ hyperfine component. For S140 HCN(1–0)

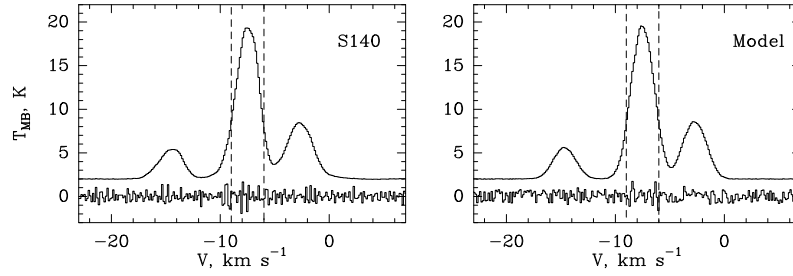


Fig. 3 The S140 HCN(1–0) profile observed with IRAM-30m (*left*) and the profile calculated in a framework of the 1D clumpy model (*right*). The residuals obtained by Fourier filtering with $F_{\text{eff}} = 1.3 \text{ (km s}^{-1}\text{)}^{-1}$ and multiplied by a factor of 40 are shown under each profile. *Dashed vertical lines* mark the range for which ΔT_{R} is calculated.

observed at IRAM-30m, the τ value is taken to be the same as for the OSO-20m observations. Yet, this value is probably underestimated. Detailed model calculations (Sect. 6) reproduce the IRAM-30m HCN(1–0) profile with $\tau \sim 1$, which lead to a ~ 2.5 times lower value of N_{tot} . The results are given in Table 2. The uncertainties of N_{tot} defined mainly by the ΔT_{R} and τ uncertainties are at least $\sim 50\%$.

6 PHYSICAL PARAMETERS OF FRAGMENTS IN S140

We used the 1D clumpy model (see Sect. 4) for detailed modeling of the HCN(1–0) profile observed in S140 at IRAM-30m (“quiet” component). The model calculations reproduce the observed HCN(1–0) profile in S140 very well (Fig. 3). By varying the density and kinetic temperature of fragments, the product of HCN abundance and the size of the cloud, and velocity dispersion of relative motions of fragments, it is possible to fit intensities of hyperfine components and widths. By varying the size of fragments and their volume filling factor, it is possible to fit the standard deviation of residual temperature fluctuations (ΔT_{R}). The observed and model profiles and the residuals after Fourier filtering with $F_{\text{eff}} = 1.3 \text{ (km s}^{-1}\text{)}^{-1}$ multiplied by a factor of 40 are shown in Figure 3. We added synthetic noise to the model profile with dispersion equal to the observed one.

The model parameters of fragments are the following: $T_{\text{KIN}} = 30 \text{ K}$, number density is $1.5 \times 10^6 \text{ cm}^{-3}$, and the size and volume filling factor of fragments are $\sim 40 \text{ a.u.}$ and ~ 0.014 , respectively. The optical depth of the central component ($F = 2 - 1$) is about 1. The total number of fragments is $\sim 2 \times 10^6$. This is comparable with the analytical estimate for HCN(1–0) in S140 observed with IRAM-30m (Table 2) if one takes $\tau = 1$.

7 DISCUSSION

New high sensitivity observations of the cores S140 and S199 confirmed the existence of residual intensity

fluctuations on line profiles found previously (Pirogov & Zinchenko 2008; Pirogov et al. 2012). Using a new method of Fourier filtering and comparing the data with the results of detailed calculations of the HCN and HCO^+ excitation in a framework of the clumpy model, it is shown that intensity fluctuations can be associated with a large number of randomly distributed identical thermal fragments moving randomly with respect to each other with suprathreshold velocities.

The total number of fragments in the beam for S140 derived from the IRAM-30m HCN(1–0) data and from the OSO-20m data agree with each other if one takes $\tau = 1$ for the IRAM-30m data. The same value derived from the $\text{HCO}^+(1-0)$ data is several times higher (Table 2). This could imply the existence of interfragment gas of lower density which effectively absorbs the HCO^+ emission and reduces the corresponding ΔT_{R} value. In order to verify this assumption, calculations in a framework of the model with interfragment gas are needed. So far, the value $\sim 4 \times 10^6$ is assumed as a reasonable estimate for the total number of thermal fragments in S140. The uncertainty of this estimate is at least 50%. Following the analysis from Pirogov & Zinchenko (2008), it can be shown that such fragments are unstable and short-lived density enhancements which most probably arise due to turbulence in high-mass star-forming cores.

The differences between the new and previous (Pirogov & Zinchenko 2008) results for S140 and S199 are connected mainly with a new method of estimating ΔT_{R} based on the regression analysis while the previous estimates were based on Fourier filtering at an arbitrarily chosen value of $F_{\text{eff}} = 0.7$. The difference in line ranges for which ΔT_{R} has been calculated and the difference in τ also increases the value of the total number of fragments in S199.

In general, the considered model is oversimplified and the estimates obtained should be treated as mean values for the regions with linear sizes $\sim 0.1 - 0.3 \text{ pc}$ in the considered cores. More realistic models should

Table 2 Total Number of Thermal Fragments in the Beam

Source	Line	ΔT_R (K)	T_R (K)	τ	T_{KIN} (K)	N_{tot}
S140 OSO-20m	HCN(1–0)	0.023	15.9(0.1)	0.15(0.04)	30	$\sim 4 \times 10^6$
S140 IRAM-30m	HCN(1–0)	0.017	17.6(0.1)			$\sim 10^7$
S140 OSO-20m	HCO ⁺ (1–0)	0.013	21.9(0.1)	0.42(0.04)		$\sim 2 \times 10^7$
S199(0,0) IRAM-30m	HCN(1–0)	0.016	8.0(0.1)	0.7(0.2)	30	$\sim 10^6$

be implemented which would combine 3D molecular line radiation transfer in a clumpy medium (e.g. Juvela 1997; Park & Hong 1998) with inhomogeneous turbulent cloud structures following from modern magnetohydrodynamics models (e.g. Haugbølle et al. 2018). On the other hand, a possibility to resolve the considered small-scale structure by an interferometer is not straightforward (interferometric observations usually reveal compact objects in the field of view, but miss more diffuse and extended emission (see, e.g., Maud et al. 2013; Palau et al. 2018)). Long-term observations with high angular resolutions using single-dish telescopes still seem to be important to search for intensity fluctuations on line profiles. An increasing sensitivity of modern receivers and implementation of new broadband spectrometers make it possible to detect residual intensity fluctuations on line profiles of various molecules in a reasonable time for different positions in objects, which together with modeling results should help to get more information about their small-scale spatial and kinematic structure.

8 CONCLUSIONS

Long-term observations of the high-mass star-forming cores S140 and S199 in HCN(1–0) and HCO⁺(1–0) lines were carried out. In order to detect intensity fluctuations on line profiles that could be due to their inner small-scale structure, the profiles were processed by the Fourier filtering method. The residual fluctuations of line radiation temperature imply the existence of a large number of randomly moving thermal fragments in the objects. Using the analytical method, the total number of fragments was calculated as being $\sim 4 \times 10^6$ for the region with linear size ~ 0.1 pc in S140 and $\sim 10^6$ for the region with linear size ~ 0.3 pc in S199. Physical parameters of thermal fragments in S140 were obtained from detailed modeling of the HCN excitation in the framework of the clumpy model including their density ($\sim 1.5 \times 10^6 \text{ cm}^{-3}$), size (~ 40 a.u.) and volume filling factor (~ 0.014). Such fragments should be unstable and short-lived objects and are probably connected with an enhanced level of turbulence in the core.

Acknowledgements I am grateful to the anonymous referee for critical reading of the manuscript, valuable com-

ments and questions which improved the paper. I would like to thank Olga Ryabukhina for help in the OSO-20m observations. I would also like to thank Igor Zinchenko for helpful discussions. The OSO-20m observations and preparation of the paper were done under support of the RFBR grants (projects 15–02–06098, 16–02–00761 and 18–02–00660). Data processing and analysis were done under support of the Russian Science Foundation grant (project 17–12–01256).

References

- Bergin, E. A., Snell, R. L., & Goldsmith, P. F. 1996, *ApJ*, 460, 343
- Guilloteau, S., & Baudry, A. 1981, *A&A*, 97, 213
- Hacar, A., Alves, J., Burkert, A., & Goldsmith, P. 2016, *A&A*, 591, A104
- Haugbølle, T., Padoan, P., & Nordlund, Å. 2018, *ApJ*, 854, 35
- Hirota, T., Ando, K., Bushimata, T., et al. 2008, *PASJ*, 60, 961
- Juvela, M. 1997, *A&A*, 322, 943
- Kamegai, K., Ikeda, M., Maezawa, H., et al. 2003, *ApJ*, 589, 378
- Kwan, J., & Sanders, D. B. 1986, *ApJ*, 309, 783
- Lim, B., Sung, H., Kim, J. S., Bessell, M. S., & Karimov, R. 2014, *MNRAS*, 438, 1451
- Malafeev, S. Y., Zinchenko, I. I., Pirogov, L. E., & Johansson, L. E. B. 2005, *Astronomy Letters*, 31, 239
- Martin, H. M., Sanders, D. B., & Hills, R. E. 1984, *MNRAS*, 208, 35
- Maud, L. T., Hoare, M. G., Gibb, A. G., Shepherd, D., & Indebetouw, R. 2013, *MNRAS*, 428, 609
- Palau, A., Zapata, L. A., Román-Zúñiga, C. G., et al. 2018, *ApJ*, 855, 24
- Park, Y.-S., & Hong, S. S. 1998, *ApJ*, 494, 605
- Pirogov, L. 1999, *A&A*, 348, 600
- Pirogov, L. E., & Zinchenko, I. I. 2008, *Astronomy Reports*, 52, 963
- Pirogov, L. E., Zinchenko, I. I., Johansson, L. E. B., & Yang, J. 2012, *Astronomical and Astrophysical Transactions*, 27, 475
- Samus, N. N., & Li, Y., *RAA (Research in Astronomy and Astrophysics)*, 2018, 18, 88
- Tachihara, K., Saigo, K., Higuchi, A. E., et al. 2012, *ApJ*, 754, 95
- Tan, J. C., Beltrán, M. T., Caselli, P., et al. 2014, *Protostars and Planets VI*, 149
- Tauber, J. A. 1996, *A&A*, 315, 591
- White, G. J., & Padman, R. 1991, *Nature*, 354, 511
- Zinchenko, I., Henning, T., & Schreyer, K. 1997, *A&AS*, 124, 385